https://doi.org/10.5194/nhess-2022-111
Preprint. Discussion started: 11 April 2022


Natural Hazards and Earth System Sciences
Discussions

# How uncertain are precipitation and peakflow estimates for the July 2021 flooding event?

Mohamed Saadi[1,2], Carina Furusho-Percot[1,2], Alexandre Belleflamme[1,2], Ju-Yu Chen[3], Silke Trömel[3,4], Stefan Kollet[1,2]

[1]Institute for Bio- and Geosciences (IBG-3, Agrosphere), Forschungszentrum Jülich, Jülich 52425, Germany
[2]Centre for High-Performance Scientific Computing in Terrestrial Systems, Geoverbund ABC/J, Jülich 52428, Germany
[3]Institute for Geosciences, Department of Meteorology, Universität Bonn, Bonn 53121, Germany
[4]Laboratory for Clouds and Precipitation Exploration, Geoverbund ABC/J, Bonn 53121, Germany

*Correspondence to*: Mohamed Saadi (m.saadi@fz-juelich.de)

**Abstract.** The disastrous July 2021 flooding events made us question the ability of current hydrometeorological tools in providing timely and reliable flood forecasts. This is an urgent concern since extreme events are increasing due to global warming. For the July 2021 events, we simulated the hourly streamflows of seven catchments in western Germany, by combining five, partly polarimetric, radar-based quantitative precipitation estimates (QPE) with two hydrological models: a conceptual lumped model (GR4H) and a physically-based, 3D distributed model (ParFlowCLM). GR4H parameters were calibrated with emphasis on high flows using historical discharge observations, whereas ParFlowCLM parameters were estimated based on landscape and soil properties. The key results are as follows: (1) All radar-based QPE products underestimated the total precipitation depth relatively to rain gauges due to intense collision-coalescence processes near the surface, i.e. below the height levels monitored by the radars. (2) The use of polarimetric radar variables led to clear improvements compared to reflectivity-based QPE products. (3) The probability of exceeding the highest measured peakflow before July 2021 was highly impacted by the QPE product, and depended on the catchment for both models. (4) The estimation of model parameters had a larger impact than the choice of QPE product, but simulated peakflows of ParFlowCLM agreed with those of GR4H for five of the seven catchments. This study highlights the need for the correction of vertical profiles of reflectivity and other polarimetric variables near the surface to improve radar-based QPE for extreme floods. It also underlines the large uncertainty in peakflow estimates due to model parameter estimation.

## 1 Introduction

### 1.1 Old questions in the light of new extremes

Many parts of the world will face an increase in the frequency and intensity of heavy summer precipitations under a warmer climate, as a result of the enhanced moisture-holding capacity of the atmosphere (Fowler et al., 2021; Kendon et al., 2014; Trenberth, 2011). This implies more frequent and flashier flood events (Dougherty and Rasmussen, 2020), hence increasing

https://doi.org/10.5194/nhess-2022-111
Preprint. Discussion started: 11 April 2022



damages to infrastructures and human losses (Dottori et al., 2018; Nissen and Ulbrich, 2017). The flooding events of July 2021 in Europe resulted in more than 220 deaths (Deutsche Welle, 2021) and costed up to €5.5 billion in insured losses, making them the most severe natural disaster caused by heavy rain and flooding in Germany (GDV, 2021). Predicting such never-seen-before extremes challenges our forecasting chains (Hapuarachchi et al., 2011) and gives a new opportunity to re-examine persistent questions: how accurate are new, state-of-the-art radar-based precipitation estimates for this event? Given the recent developments in radar-based precipitation estimation and hydrological modeling, which of these sources of uncertainty is prevalent in extreme peakflow estimation?

### 1.2 Precipitation estimates and hydrological modeling approaches

Rain gauges are often used as a reference source of quantitative precipitation estimates (QPE; Boushaki et al., 2009; Derin et al., 2019; Dumont et al., 2022; Schleiss et al., 2020). However, they are sparse and may miss the spatial variability of precipitation, especially of convective precipitation fields that can generate extreme flooding events in high-elevation, complex terrain configurations (Anquetin et al., 2005; Emmanuel et al., 2017; Sokol et al., 2021; Tetzlaff and Uhlenbrook, 2005). Alternatively, operational radar-based QPE provide better coverage and characterization of precipitation dynamics with higher spatial and temporal resolutions, which is particularly useful for flooding events (Anagnostou et al., 2010; Zhou et al., 2017). Traditionally, radar-based QPE are derived from horizontal reflectivity ($Z_h$) using Marshall-Palmer-type formulae (Marshall and Palmer, 1948). However, they are highly sensitive to the variability of the raindrop size distribution, and in some cases, QPE based on $Z_h$ only tend to underestimate heavy precipitation (Harrison et al., 2000; Park et al., 2019; Schleiss et al., 2020). In addition, they are affected by radar calibration, attenuation, partial beam blockage, and radome effect (Berne and Krajewski, 2013; Borga et al., 2007; Chen et al., 2021; Diederich et al., 2015a, b; Ryzhkov et al., 2014). These limitations can be overcome by using additional variables from dual-polarimetric radars, which provide a better characterization of the shape and the concentration of hydrometeors and are less sensitive to raindrop size distribution (Gourley et al., 2010; Ryzhkov et al., 2005). Phase-based observables from polarimetric radars, such as specific differential phase ($K_{DP}$) and specific attenuation at horizontal/vertical polarization ($A_{H/V}$), help improve QPE especially for heavy, convective and hail-contaminated rainfall events (Anagnostou et al., 2018; Berne and Krajewski, 2013; Chen et al., 2021; Ryzhkov et al., 2014). However, including these variables may only lead to better spatial correlations with limited improvements in biases (Cunha et al., 2015). These improvements in radar-based QPE have been commonly evaluated with regards to point-scale ground-based measurements, but when the ultimate goal is to provide an accurate estimation of flood severity, a catchment-scale hydrological evaluation is needed.

Precipitation is the main driving factor of land-surface hydrological processes at the event-scale. Consequently, uncertainties in the input QPE strongly control the uncertainties of hydrological model outputs (Oudin et al., 2006; Renard et al., 2011), and are found to be larger than structural uncertainties of the models (Kuczera et al., 2006; Zappa et al., 2011). Previous studies evaluated the added value of improved spatial and temporal resolutions of QPE using hydrological models. Cole and Moore (2009) showed the benefits of gauge-corrected radar-based QPE for ungauged locations using a distributed

https://doi.org/10.5194/nhess-2022-111
Preprint. Discussion started: 11 April 2022




hydrological model. Lobligeois et al. (2014) found that using high-resolution, spatially-distributed precipitation was mainly beneficial in regions with high spatial variability of precipitation and topography fields. For flash flood applications, several studies (e.g., Borga et al., 2007; Braud et al., 2010; Emmanuel et al., 2017; Lin et al., 2018) concluded that QPE are the major controlling factor of flash flood dynamics and of hydrological model performances. However, they found that the extent to which uncertainties in QPE impacted model outputs is dependent on the strength of the storage behavior of the catchment, which may hide the benefit of using high-resolution QPE (Pokhrel and Gupta, 2011). Yet, fewer studies (e.g., Gourley et al., 2010; He et al., 2018) assessed the added-value of polarimetric radar measurements to predicting hydrological extremes. Additionally, the reliability of calibrated models for predicting unprecedented extreme hydrological events is questionable as they depend on historical observations (Poméon et al., 2020). In this respect, little attention has been drawn to how highly contrasted model formulations (lumped, conceptual vs. distributed, physically-based) are affected by uncertainties in QPE inputs for the case of extreme precipitation events.

### 1.3 Insights from the disastrous July 2021 events in western Germany

This study investigated the influence of improved QPE and different representations of hydrological processes on the uncertainties in simulating extreme flooding events. The novelties of our study consist in: (1) using new QPE products from phase-based observables of C-band radars, (2) contrasting hydrological modeling approaches (conceptual vs. partial differential equations (PDE)-based model), and (3) proposing an evaluation framework of the hydrometeorological prediction chain for unprecedented extreme events with unavailable discharge measurements. Since no peakflow measurements are available (partly due to destroyed monitoring systems), our analysis focused on the probability that the simulated peakflow exceeds the highest historically observed peakflow. This is relevant because hydrological models are often evaluated based on their ability to detect the probability of flows exceeding catchment-specific, critical thresholds for flood warning applications (Anctil and Ramos, 2017).

This paper is structured as follows: Sect. 2 presents the studied region, Sect. 3 explains the methodology, Sect. 4 and 5 show and discuss our results, and Sect. 6 summarizes our conclusions.

## 2 Study region

Our study focused on a set of seven catchments located in western Germany (Fig. 1a), draining parts of the Eifel low-mountain range, with areas ranging between 144 and 1670 km$^2$ (Table 1). Four of the seven stream gauges are located on the Ahr and the Kyll rivers in the federal state of Rhineland-Palatinate. The remaining three stream gauges are located on the Erft and Rur rivers in the federal state of North Rhine-Westphalia. Their hypsometry shows a rolling plateau at mild elevations (300 m to 700 m) except for the catchments drained by the Erft river (Fig. 1b). Their land cover is dominated by agricultural and forest areas, with relatively small proportion of artificial areas (Table 1). Average precipitation depths range from 700 mm $yr^{-1}$ to 1080 mm $yr^{-1}$ and corresponding aridity indices are between 0.5-0.9, which reflects a region with temperate climate under oceanic influence.

## 3 Methodology

### 3.1 The lumped conceptual hydrological modeling approach

We selected GR4H (Ficchì et al., 2019) as a representative of the lumped, conceptual modeling approach. GR4H inputs consist of catchment-average precipitation and potential evapotranspiration at the hourly timestep. Potential evapotranspiration was estimated using a formula based on catchment-average temperature. GR4H estimates net precipitation from input precipitation using an interception with a soil-moisture accounting reservoir. Then, the net precipitation is split into 10 % routed through the quick-flow routing branch (via a unit hydrograph) and 90 % routed through the slow-flow branch (via a unit hydrograph and a nonlinear routing reservoir). On both branches, exchanges between surface water and groundwater are enabled. Detailed equations can be found in Ficchì et al. (2019) and Perrin et al. (2003).

We calibrated GR4H parameters using historical observations of discharge and a gradient-descent based algorithm (Coron et al., 2017; Edijatno et al., 1999). Since hourly discharge values for all stream gauges were unavailable, hourly model simulations were aggregated into daily time steps to be compared to the daily discharge observations. Because we are interested in simulating high discharge values, we looked for optimal parameters $\theta_{opt}$ that maximized the following objective function $FO(\theta)$:

$$FO(\theta) = \frac{1}{4} C(Q_{sim}(\theta), Q_{obs}) + \frac{3}{4} C\left(Q_{sim}(\theta), Q_{obs} | Q_{obs} \geq Q_{obs,th}\right) \tag{1}$$

where $\theta$ are model parameters, $Q_{sim}(\theta), Q_{obs}$ are respectively simulated and observed discharges, $C(Q_{sim}(\theta), Q_{obs})$ is a calculated error criterion over the whole period of calibration, and $C\left(Q_{sim}(\theta), Q_{obs} | Q_{obs} \geq Q_{obs,th}\right)$ is calculated only for periods when the observed discharge is above the threshold $Q_{obs,th}$, which emphasizes high flows. To account for the uncertainties in parameter estimation, we split the available time series into two distinct and length-equivalent sub-periods (2007-2013 and 2014-2020), over which we calibrated the model with regards to two criteria $C$: the Nash-Sutcliffe Efficiency (Nash and Sutcliffe, 1970) and the Kling-Gupta Efficiency (Gupta et al., 2009). For the threshold $Q_{obs,th}$, we chose three values: the minimum discharge value (i.e., no particular emphasis on high flows), the 90$^{th}$ percentile, and the 99$^{th}$ percentile of daily discharge values. Combining these choices yielded 2*2*3 = 12 optimal parameter sets for each catchment. During calibration, the first year of records (2006) was used for model spin-up to minimize the impact of model initialization on model calibration and simulation results.

### 3.2 The distributed PDE-based hydrological modeling approach

In addition to GR4H, we used the hydrological model ParFlow with its internal land surface module CLM (Common Land Model), hereafter ParFlowCLM (Kollet and Maxwell, 2006; Kuffour et al., 2020; Maxwell, 2013), implemented on a 611-m

https://doi.org/10.5194/nhess-2022-111
Preprint. Discussion started: 11 April 2022


Natural Hazards and Earth System Sciences Discussions
Open Access

resolution grid with 15 depth layers down to 60 m below the surface, with geometrically increased thickness. CLM resolves the energy budget at the land surface as well as the water exchange at the atmosphere-land-soil interface, which helps discern the net precipitation from interception, soil evaporation, plant transpiration, and infiltration. ParFlow resolves the 3D Richards' equation for variably saturated subsurface and groundwater flow, coupled with the kinematic wave model for the overland flow routing. Assuming the continuity of pressure at the ground surface, the boundary fluxes for Richards' equation are estimated from the kinematic wave model, and vice versa (Kollet and Maxwell, 2006). The model represents both the Hortonian and the Dunne runoff processes, and it accounts for exfiltration and re-infiltration at the downstream hydraulic pathway.

ParFlowCLM was forced at the hourly time step with a spin-up period starting from 2007. Slopes were estimated from the ASTER (Advanced Spaceborne Thermal Emission and Reflection Radiometer; https://lpdaac.usgs.gov/products/astgtmv003) DEM (digital elevation model) combined with the hydrologically-enhanced DEM MERIT Hydro (Yamazaki et al., 2019). Soil and subsoil types are defined from the SoilGrids250m (Hengl et al., 2017) reclassified into 12 USDA (United States Department of Agriculture) texture types. The hydraulic parameters for each soil type (hydraulic conductivity, residual and saturated water content, and van Genuchten parameters) were obtained from the ROSETTA model (Schaap et al., 2001). Below the depth to bedrock, given by SoilGrids250m, the typology of the International Hydrogeological Map of Europe IHME1500 (scale 1:1500000) was used (Duscher et al., 2015). Land cover was characterized using the CORINE Land Cover database of the Copernicus Land Monitoring Service for the year 2018 (Langanke et al., 2016), whose land cover classification was converted into the 18 IGBP (International Geosphere-Biosphere Programme) categories. To account for the uncertainty in Manning's roughness coefficient, which highly impacts the peakflow simulations (Lumbroso and Gaume, 2012), three uniformly distributed values were tested for the whole domain: a default value of 0.2 s $m^{-1/3}$ (HMann, i.e. high roughness, from Schalge et al., 2019), and two additional values of 0.1 s $m^{-1/3}$ (MMann, medium roughness) and 0.02 s $m^{-1/3}$ (LMann, i.e. low roughness). These three values cover the whole range of Manning's coefficient values reported by Lumbroso and Gaume (2012).

### 3.3 Atmospheric forcing and streamflow data

Eight atmospheric variables were needed for the runs of ParFlowCLM, namely 2-m air temperature, precipitation, surface pressure, downward solar and thermal radiation, specific humidity, and eastward and northward components of the 10-m wind. Precipitation was obtained from the operational radar-based RADOLAN product of the DWD (*Deutsche Wetterdienst*, German Weather Service), which is gauge adjusted and available at 1-km resolution. The remaining atmospheric variables were obtained from the ERA5-Land dataset (Muñoz-Sabater et al., 2021), available at 9-km resolution. All variables were regridded to the model resolution using a bicubic interpolation. For GR4H, data demand is limited to precipitation and 2-m air temperature, which were catchment-averaged using the Thiessen polygon method, and discharge data for model calibration, which were obtained for the period 2007-2021 from the state offices for environment of North Rhine-Westphalia (LANUV, https://www.elwasweb.nrw.de) and Rhineland-Palatinate (https://wasserportal.rlp-umwelt.de).

https://doi.org/10.5194/nhess-2022-111
Preprint. Discussion started: 11 April 2022



### 3.4 Evaluation of QPE products and modeling choices for the July 2021 events

For the 14 July 2021, we tested five radar-based, 1-km gridded QPE products as detailed in Table 2. These products were derived from the measurements of polarimetric radars operated by DWD using algorithms that exploit horizontal reflectivity ($Z_h$), specific differential phase ($K_{DP}$), and specific attenuation at horizontal ($A_H$) and vertical ($A_V$) polarization (Chen et al., 2021). We evaluated the radar-based QPE first with respect to their agreement with rain gauges both at the point scale and at the catchment scale, and then with respect to their effect on simulated peakflows by GR4H and ParFlowCLM.

First, total rainfall depths for the 14 July 2021 of the radar-based QPE are compared at the point scale with the rain gauges using the normalized root-mean-square error ($nRMSE$), the normalized mean bias ($NMB$), and the Pearson's correlation coefficient ($CC$), expressed as:

$$\begin{cases} nRMSE(\%) = 100 \cdot \dfrac{\sqrt{\sum_{i=1}^{N}(P_{radar,i} - P_{RG,i})^2}}{\sqrt{\sum_{i=1}^{N}(\overline{P_{RG}} - P_{RG,i})^2}} \\ NMB(\%) = 100 \cdot \dfrac{\sum_{i=1}^{N}(P_{radar,i} - P_{RG,i})}{\sum_{i=1}^{N} P_{RG,i}} \\ CC = \dfrac{\sum_{i=1}^{N}(P_{RG,i} - \overline{P_{RG}})(P_{radar,i} - \overline{P_{radar}})}{\sqrt{\sum_{i=1}^{N}(P_{RG,i} - \overline{P_{RG}})^2 \sum_{i=1}^{N}(P_{radar,i} - \overline{P_{radar}})^2}} \end{cases} \tag{2}$$

where $P_{RG,i}$ is the total rainfall depth for the 14 July 2021 measured at the $i^{th}$ rain gauge, $P_{radar,i}$ is the total rainfall depth given by the radar-based QPE rad (Table 2) and averaged over the raster cell containing the $i^{th}$ rain gauge and its 8 neighbouring cells, and $\overline{P_{RG}}$, $\overline{P_{radar}}$ are the averages of total rainfall depths of the considered $N$ rain gauges and their corresponding $N$ averages from neighbouring raster cells of the radar-based QPE, respectively. $nRMSE$ and $NMB$ have both a perfect score of 0, and $CC$ has a perfect score of 1. Positive $NMB$ indicate that the radar-based QPE overestimates the total rainfall depth for the 14 July 2021 compared to rain gauges, and vice versa.

At the catchment scale, the spatial average QPE from radar for the 14 July 2021 is compared with that from rain gauges using the relative error:

$$\Delta_{rel}(P_{radar}, P_{RG})(\%) = 100 \cdot \frac{P_{radar} - P_{RG}}{P_{RG}} \tag{3}$$

which is positive (respectively negative) when radar-based QPE overestimates (respectively underestimates) the total catchment-average precipitation depth with respect to rain gauges, and equals zero for a perfect match.

Second, we examined the effect of QPE on the frequency of exceeding the highest historically observed peakflow for each catchment (Table 1) by simulated peakflows, which consist of 12 simulations of GR4H in addition to three simulations of ParFlowCLM. Although GR4H simulations predominate, this will still illustrate the effect of QPE input on how well a model can issue a warning of an upcoming event that has never been seen before.

Third, for each catchment and for each model, the effect of the choice of QPE input is analyzed using the relative error in simulated peakflows attributed to replacing RADOLAN with another QPE product, such as:

https://doi.org/10.5194/nhess-2022-111
Preprint. Discussion started: 11 April 2022



$$\Delta_{rel}Q_{p,sim}(QPE, RADOLAN)(\%) = 100 \cdot \frac{Q_{p,sim}(QPE) - Q_{p,sim}(RADOLAN)}{Q_{p,sim}(RADOLAN)} \quad (4)$$

which is positive (respectively negative) if using QPE products other than RADOLAN leads to higher (respectively lower) simulated peakflows. Similarly, agreement across all QPE products between GR4H and ParFlowCLM is estimated using:

$$\Delta_{rel}Q_{p,sim}(GR4H, ParFlowCLM)(\%) = 100 \cdot \frac{Q_{p,sim,GR4H} - Q_{p,sim,ParFlowCLM}}{Q_{p,sim,ParFlowCLM}} \quad (5)$$

where $Q_{p,sim,GR4H}$ and $Q_{p,sim,ParFlowCLM}$ are simulated peakflows by GR4H and ParFlowCLM, respectively. Perfect agreement is obtained with a relative error equal to zero, whereas positive (respectively negative) values indicate that GR4H overestimates (respectively underestimates) peakflows compared to ParFlowCLM. This relative error is estimated using all possible combinations of the 12 estimated peakflows of GR4H and the three estimated peakflows of ParFlowCLM.

## 4 Results

### 4.1 Point-scale and catchment-scale differences between the QPE product

The different radar-based QPE show a relatively similar spatial pattern to rain gauges, as can be seen in Fig. 2. Heavy precipitation depths have fallen over the highest altitudes, namely the Eifel range on the left bank of the Rhine river and the Bergisches Land on the right bank. These rainfall depths were a result of long-lasting intense stratiform rain connected to a cut-off low pressure system (Junghänel et al., 2021), which locally broke historical precipitation records (Kreienkamp et al., 2021). For the rain gauge measurements, precipitation depths reached up to 162 mm, which is equivalent to what would fall in 2-3 months on average. Conversely, the radar products significantly differ in terms of total precipitation depth for the 14 July. QPE based on specific attenuation (RAHKDP and RAVKDP) showed higher precipitation depths compared to RADOLAN, whereas QPE based on horizontal reflectivity (RZH and RZHKDP) showed quite low precipitation depths.

At the point scale, the comparison with $N$ = 67 rain gauges over the region shows RADOLAN to be the radar-based QPE that agrees most with the rain gauges (Fig. 3). Values of $nRMSE$ varied from 32 % for RADOLAN to 37-39 % for the two products based on specific attenuation (RAHKDP and RAVKDP), and then jumped to 47-49 % for the remaining radar-based QPE (RZHKDP and RZH). The negative $NMB$ values show that all products underestimated the precipitation amounts compared to rain gauges, but this underestimation remains below 15 % for RADOLAN, RAVKDP and RAHKDP. $NMB$ values confirm the relatively high biases obtained with RZHKDP and RZH, for which underestimation was over 20 %. Nevertheless, the high $CC$ values confirm that all products captured well the spatial pattern of the ground-based precipitation measurements.

Conclusions about the agreement between QPE products and rain gauges change when we look at the catchment scale evaluation. Specifically, QPE based on specific attenuation outperformed RADOLAN across the seven catchments (Fig. 4), and reduced relative error from a median of -18 % for RADOLAN to -6 % for RAHKDP. Nevertheless, all products underestimated catchment-scale precipitation with respect to rain gauges, confirming the point-scale results (see $NMB$ scores in Fig. 3). This comparison underlines the fact that the assessment of QPE products is catchment-dependent. QPE based on specific attenuation outperformed RADOLAN for the catchments drained by the Ahr, the Kyll, and the Erft at Bliesheim, whereas RADOLAN was the only product that agreed with rain gauges for the Rur at Monschau. However, all radar-based QPE underestimated the precipitation depth obtained on rain gauges for the largest catchment, the Erft at Neubrueck.

### 4.2 Effect of QPE and modeling choices on simulated peakflows

The QPE inputs significantly impacted both GR4H and ParFlowCLM model simulations, as illustrated in Fig. 5 for the Ahr at Altenahr. Changing from RADOLAN to RAVKDP led to increased peakflow simulations, which is in line with the catchment-scale comparison (Fig. 4). For this catchment, a relative agreement was reached between the two models as GR4H simulations bracketed ParFlowCLM simulations, except for the case when the Manning's coefficient was the lowest (LMann). Both the choices of GR4H calibration and Manning's coefficient led to high uncertainty of peakflow simulations. With a high Manning's coefficient, ParFlowCLM succeeded in estimating both the timing and the magnitude of the last recorded peakflow at the catchment outlet (~330 $m^3 s^{-1}$ at ~19:00 of the 14 July), whereas the median simulation of GR4H was quite delayed with respect to ParFlowCLM simulated hydrographs. Finally, all model simulations with both RADOLAN and RAVKDP illustrate that the heavy precipitation event resulted in a record-breaking flood for the Ahr at Altenahr.

Overall, the ranking of QPE products with respect to the total precipitation depth for the 14 July was preserved by model simulations for all catchments, as shown in Fig. 6. Specifically, the distributed approach by ParFlowCLM reflected the relative differences between catchment-average QPE. ParFlowCLM simulations with high and medium Manning's values were bracketed by those of GR4H except for the largest catchment (Erft at Neubrueck) and the smallest catchment (Rur at Monschau). However, both the distributions of simulated peakflows by GR4H and ParFlowCLM revealed a large uncertainty due to model parameter estimation. For instance, simulated peakflows by GR4H for the Ahr at Altenahr varied between 150-850 $m^3 s^{-1}$ using RZH as input, whereas they varied between 330-1360 $m^3 s^{-1}$ using RAHKDP as input.

The exceedance frequency of the highest peakflow ever measured (orange dashed lines in Fig. 6) by model simulations was impacted by QPE inputs depending on the catchment (Fig. 7). The first subset of catchments, including the Ahr catchments and the Erft at Bliesheim, showed high chances of breaking the records with little or no impact of QPE inputs. Similarly, for the Rur at Monschau, all model simulations from the different QPE products agreed that the event was not heavy enough to surpass the highest measured peakflow. The second subset (Erft at Neubrueck and Kyll) showed different answers to whether there was a high chance (i.e., more than 50 %) that the event peakflow will overpass the highest measured peakflow before the event. In particular, simulations with the operational RADOLAN product for the Kyll at Kordel gave lower chances than 50 % compared to rain gauges and products based on specific attenuation. This subset of catchments underlines the crucial impact of the input QPE on our interpretation of the severity of the event.

In general, the differences between simulated peakflows seemed to be more influenced by the model parametrization than the choice of the QPE input, as suggested by Fig. 8. GR4H tended to underestimate the event peakflow relatively to ParFlowCLM, and both models disagreed most in the Erft at Neubrueck and the Rur at Monschau. The differences between GR4H and ParFlowCLM were generally independent of the QPE input (Fig. 8a). Conversely, replacing RADOLAN with

https://doi.org/10.5194/nhess-2022-111
Preprint. Discussion started: 11 April 2022



any other QPE led to systematic increases in simulated peakflows (except for the Rur at Monschau) with error distributions less far from zero (Fig. 8b). GR4H showed higher sensitivity to QPE products compared to ParFlowCLM, which suggests that the distributed model smoothed more the differences between QPE products.

## 5 Discussion

### 5.1 Importance of hydrological, catchment-scale evaluation of QPE products

Our evaluation shows that the radar-based QPE agreed with rain gauges in terms of spatial pattern (Fig. 2, $CC$ values in Fig. 3), which endorses that their use for a denser spatial characterization of precipitation fields is needed. Conversely, all radar-based QPE still suffer from important underestimation of heavy precipitation relative to rain gauges, in particular for QPE relying only on horizontal reflectivity $Z_h$. In a study over four countries, Schleiss et al. (2020) found that radar products underestimated heavy rain compared to rain gauges by up to 44%, and Park et al. (2019) found that the pan-European radar composites OPERA systematically underestimated daily precipitation compared to rain gauges. For the 14 July 2021 event, this underestimation may be explained by intense collision-coalescence processes taking place close to the surface, i.e. mostly below the height levels monitored by the radars. With increasing distance from the site, radars scan at increasing heights. As a consequence, a nearly complete vertical profile of radar-measured variables is available in the vicinity of the different radar sites, but not area-wide. To overcome the resulting deficiencies for radar-based QPE, the spatiotemporal variability of radar profiles available at the different sites needs to be exploited for an area-wide correction of the vertical profiles in further steps.

Apart from the need for the correction of vertical profiles, Fig. 2 and Fig. 4 demonstrate the benefit of using polarimetric radar variables, such as specific attenuation and specific differential phase, to improve the QPE with respect to rain gauges, especially in extreme rainfall events (Gourley et al., 2010). However, the improvements relative to RADOLAN, which is based on reflectivity and rain-gauges adjusted, could only be demonstrated at the catchment scale. Model simulations by GR4H and especially by the distributed ParFlowCLM (Fig. 4-8) are coherent with the catchment-scale evaluation of Fig. 3, which suggests that the widely applied point-scale evaluation (e.g., Chen et al., 2021; Derin et al., 2019; Schleiss et al., 2020) may not be thorough enough for hydrological applications.

The sensitivity of model simulations confirms the dominant impact of QPE on hydrological model performances (Braud et al., 2010; Oudin et al., 2006), underlining the need for reliable precipitation estimates especially for extreme flooding events. However, the effect of QPE was relatively smaller than that of parameter estimation, and it was variable from one catchment to another for the 14 July event (Fig. 6-7). This indicates that the differences (particularly the improvements) may be filtered out depending on the catchment properties (size and shape), the spatial variability of antecedent moisture conditions and the precipitation fields (Lin et al., 2018; Pechlivanidis et al., 2016; Pokhrel and Gupta, 2011; Saulnier and Le Lay, 2009). Antecedent soil moisture conditions may indeed be a high factor in the variability of the impact of QPE on the

https://doi.org/10.5194/nhess-2022-111
Preprint. Discussion started: 11 April 2022

Natural Hazards and Earth System Sciences
Discussions

severity of the floods from one catchment to another, as the 10-day (respectively 5-day) antecedent precipitations varied from 40 to 66 mm (respectively 20 to 44 mm) over the seven catchments.

### 5.2 (Dis)agreement of contrasting modeling approaches

Earlier studies focused on the difference between a distributed and a lumped approach while retaining the same complexity of process representation (e.g., Cole and Moore, 2009; Huang et al., 2019; Lobligeois et al., 2014). Our study compared contrasting modeling approaches both in terms of spatial and process representation. This follows the study of Poméon et al. (2020) that compared the 3D distributed ParFlow with the calibrated HBV model for flash flood events in Germany. Poméon et al. (2020) found that parameter estimation of HBV was highly dependent on extreme flooding events in the calibration period to achieve similar performances to ParFlow. In our study, all previous extreme floods were kept in the calibration time-series, but the strongest peakflow obtained with ParFlowCLM was still higher than the range of peakflows simulated with GR4H. The non-bracketed, high ParFlowCLM simulations associated with a low Manning's coefficient (LMann) may suggest that the tested value is perhaps too low, but it is still within the range of Manning's values from guidance documents (Lumbroso and Gaume, 2012). In addition, using a coarse model resolution should be compensated by lower Manning's coefficient values (Schalge et al., 2019). The large uncertainty due to the Manning's coefficient is perhaps accentuated by the nature of the relationship between the coefficient and the discharge, but it is still here a lower bound since uncertainty to other parameters (hydraulic conductivity, van Genuchten parameters) was not included. This underlines that even the physically-based approach does not completely overcome the issue of parameter estimation, particularly for extreme and record-breaking floods.

GR4H peakflows were delayed compared to the ones simulated by ParFlowCLM, which is perhaps related to the delaying effect of the unit hydrographs of GR4H. The base time of these unit hydrographs is lumped (i.e., catchment-averaged) and calibrated on long-term discharge records, which implies that it reflects a smoother response than the exceptional July 2021 flood development. Moreover, GR4H significantly underestimated peakflow relative to ParFlowCLM for the Erft at Neubrueck and the Rur at Monschau. In the case of the Erft at Neubrueck, we suspect that these differences are related to the strong anthropogenic intervention (flood protection systems, dominant agricultural activity; see Table 1 and Staatliches Umweltamt Köln, 2005) which could be learned by GR4H from the calibration process on historical observations, in contrast to ParFlowCLM that does not explicitly account for such anthropogenic effects. For the Rur at Monschau, the differences between simulated hydrographs by ParFlowCLM and GR4H may be due to the existence of small reservoirs at the upstream. These differences would be better understood if GR4H parameters have been estimated using information from hourly discharge measurements.

Due to the low computational cost of the GR4H implementation, estimating the uncertainty of its peakflow simulations was less demanding than with ParFlowCLM. However, using the extreme, physically possible values of Manning's parameter allowed ParFlowCLM to simulate higher peakflows than the calibrated model, suggesting that it could provide a more accurate range of possible values of unprecedented events, unlike the calibrated GR4H. One could combine both

https://doi.org/10.5194/nhess-2022-111
Preprint. Discussion started: 11 April 2022



models by running a few ParFlowCLM simulations, use GR4H with various calibration approaches to map the uncertainty in peakflow estimation from different behavioural model parameters and different climatic inputs, and then transfer this uncertainty to ParFlowCLM simulations. This would, however, require exhaustive analysis of the agreement between ParFlowCLM and GR4H for a wide variety of catchments.

### 5.3 Study limitations

First, focusing on only one event for a few catchments makes our conclusions event- and location-dependent. A large sample approach (such as in Raimonet et al., 2017; Singh and Reza Najafi, 2020) would help analyze the interplay between QPE and contrasting modeling philosophies not only for extreme event purposes, but also for overall long-term hydrological needs. Second, the absence of reliable discharge measurements for the catastrophic event limits our model evaluation, but our model simulations could be used as estimates of the severity of the flooding event, despite the large uncertainty in simulated peakflows. Third, our study overlooked the effect of distributed antecedent saturation on the evaluation of QPE, which would help explain the differences between the catchments under humid antecedent conditions. Fourth, the accuracy of the parameter estimation in our study could be improved by adopting a distributed Manning's value for the ParFlowCLM setup, investigating the uncertainty related to other distributed parameters (such as hydraulic conductivity; Poméon et al., 2020), or using hourly discharge streamflows for the GR4H calibration.

## 6 Conclusions and future work

The July 2021 events in western Germany questioned the ability of our current methods of precipitation estimation and hydrological modeling of correctly anticipating the severity of the floods. We evaluated state-of-the-art radar-based QPE and two contrasting hydrological models, the conceptual and lumped GR4H with the 3D-distributed and physically-based ParFlowCLM, to analyze how the choices of QPE or hydrological modeling approach impacted the simulated peakflows. We concluded that:

1. The different radar-based QPE products underestimated the total precipitation depth for the 14 July 2021 relatively to rain gauges, due to high variability of the vertical structure of precipitation.
2. Using phase-based variables from polarimetric radar retrievals helped improve the QPE, especially by including the specific differential phase ($K_{DP}$) combined with specific attenuation at horizontal/vertical polarization ($A_{H/V}$). These improvements were best highlighted at the catchment scale using the hydrological models, which suggests that a point-scale evaluation may not be enough for hydrological applications.
3. The QPE impacted both GR4H and ParFlowCLM simulations, but their impact on the severity of the flood (i.e., surpassing the highest historically measured peakflow) varied from one catchment to another.
4. A large uncertainty characterized the peakflow simulations by both GR4H and ParFlowCLM, but they agreed in detecting historical threshold in most catchments.

https://doi.org/10.5194/nhess-2022-111
Preprint. Discussion started: 11 April 2022


Natural Hazards and Earth System Sciences
Discussions

As future work, a larger timespan with more extreme events are to be considered to confirm these conclusions. A correction of vertical profiles of radar variables is to be implemented for further improvements of the accuracy of the QPE products. A modeling framework that combines ParFlowCLM and GR4H to better anticipate never-seen-before events is to be designed to benefit from the advantages of both modeling philosophies.

*Author contributions*. Conceptualization: MS, CFP, and SK; Data curation: MS and JYC; Formal analysis: MS; Funding acquisition: CFP, SK, and ST; Investigation: MS and CFP; Methodology: MS, CFP, and AB; Project administration: CFP, ST, and SK; Software: MS and AB; Supervision: CFP and SK; Visualization: MS; Writing – original draft: MS; Writing – review and editing: MS, CFP, AB, JYC, and ST.

*Competing interests*. The authors declare that they have no conflict of interest.

*Funding*. This study is part of the RealPEP (Near-Realtime Quantitative Precipitation Estimation and Prediction https://www2.meteo.uni-bonn.de/realpep/doku.php) P4 project (Evaluation of QPE and QPN improvements in a flash flood nowcasting framework with data assimilation), funded by the *Deutsche Forschungsgemeinschaft* (German Research Foundation). Computing resources for ParFlowCLM were provided by the Jülich Supercomputing Center (JSC).

*Code and data availability*. Both ParFlowCLM (https://parflow.org/) and GR4H (https://github.com/cran/airGR) codes are available in public repositories. All original data are public, except for the QPE products generated for the study, which can be made available upon reasonable request from the authors.

Natural Hazards and Earth System Sciences
Discussions

**Table 1:** Hydroclimatic and landscape characteristics of the seven studied catchments. Data sources are detailed in Sect. 3.3.

| River | Area (km$^2$) | Mean precipitation (mm yr$^{-1}$) | Aridity index (-) | Mean discharge (mm yr$^{-1}$) | Artificial (%) | Agricultural (%) | Forest (%) | Water bodies (%) | Highest measured peakflow before July 2021 (m$^3$ s$^{-1}$) |
|---|---|---|---|---|---|---|---|---|---|
| Ahr at Muesch | 350 | 790 | 0.75 | 280 | 4.0 | 52.9 | 43.1 | 0.0 | 132 |
| Ahr at Altenahr | 760 | 760 | 0.78 | 280 | 3.5 | 39.5 | 57.0 | 0.0 | 236 |
| Kyll at Densborn | 470 | 890 | 0.65 | 450 | 4.0 | 47.7 | 48.2 | 0.0 | 180 |
| Kyll at Kordel | 840 | 830 | 0.71 | 370 | 5.4 | 51.9 | 42.7 | 0.0 | 218 |
| Erft at Bliesheim | 550 | 700 | 0.89 | 130 | 12.6 | 59.1 | 28.2 | 0.0 | 55.8 |
| Erft at Neubrueck | 1670 | 740 | 0.86 | 180 | 17.7 | 64.3 | 17.8 | 0.2 | 46.6 |
| Rur at Monschau | 144 | 1080 | 0.52 | 760 | 6.1 | 25.4 | 62.9 | 5.6 | 109.6 |

https://doi.org/10.5194/nhess-2022-111
Preprint. Discussion started: 11 April 2022


Natural Hazards and Earth System Sciences
Open Access
Discussions

**Table 2:** Summary of QPE products tested for the 14 July 2021 for the study region.

<table>
<tr><th>QPE abbreviation</th><th>Description</th><th>Source</th><th>Run with</th></tr>
<tr><td>Rain gauges</td><td>Precipitation measurements from rain gauges</td><td>DWD (https://opendata.dwd.de)</td><td>GR4H</td></tr>
<tr><td>RADOLAN</td><td>Radar-Online-Aneichung, the operational QPE product of the DWD, adjusted to rain gauges</td><td>DWD (https://opendata.dwd.de)</td><td rowspan="5">GR4H, ParFlowCLM</td></tr>
<tr><td>RZH</td><td>Precipitation estimation based on horizontal reflectivity ($Z_h$): $R(Z_h)$</td><td rowspan="4">Chen et al. (2021)</td></tr>
<tr><td>RZHKDP</td><td>Precipitation estimation based on horizontal reflectivity ($Z_h$) when $Z_h \leq$ 40 dBZ and specific differential phase ($K_{DP}$) when $Z_h >$ 40 dBZ: $R(Z_h)/R(K_{DP})$</td></tr>
<tr><td>RAHKDP</td><td>Precipitation estimation based on specific attenuation at horizontal polarization ($A_H$) and specific differential phase ($K_{DP}$) when $Z_h >$ 40 dBZ: $R(A_H)/R(K_{DP})$</td></tr>
<tr><td>RAVKDP</td><td>Precipitation estimation based on specific attenuation at vertical polarization ($A_V$) and specific differential phase ($K_{DP}$) when $Z_h >$ 40 dBZ: $R(A_V)/R(K_{DP})$</td></tr>
</table>

https://doi.org/10.5194/nhess-2022-111
Preprint. Discussion started: 11 April 2022


Natural Hazards and Earth System Sciences
Discussions

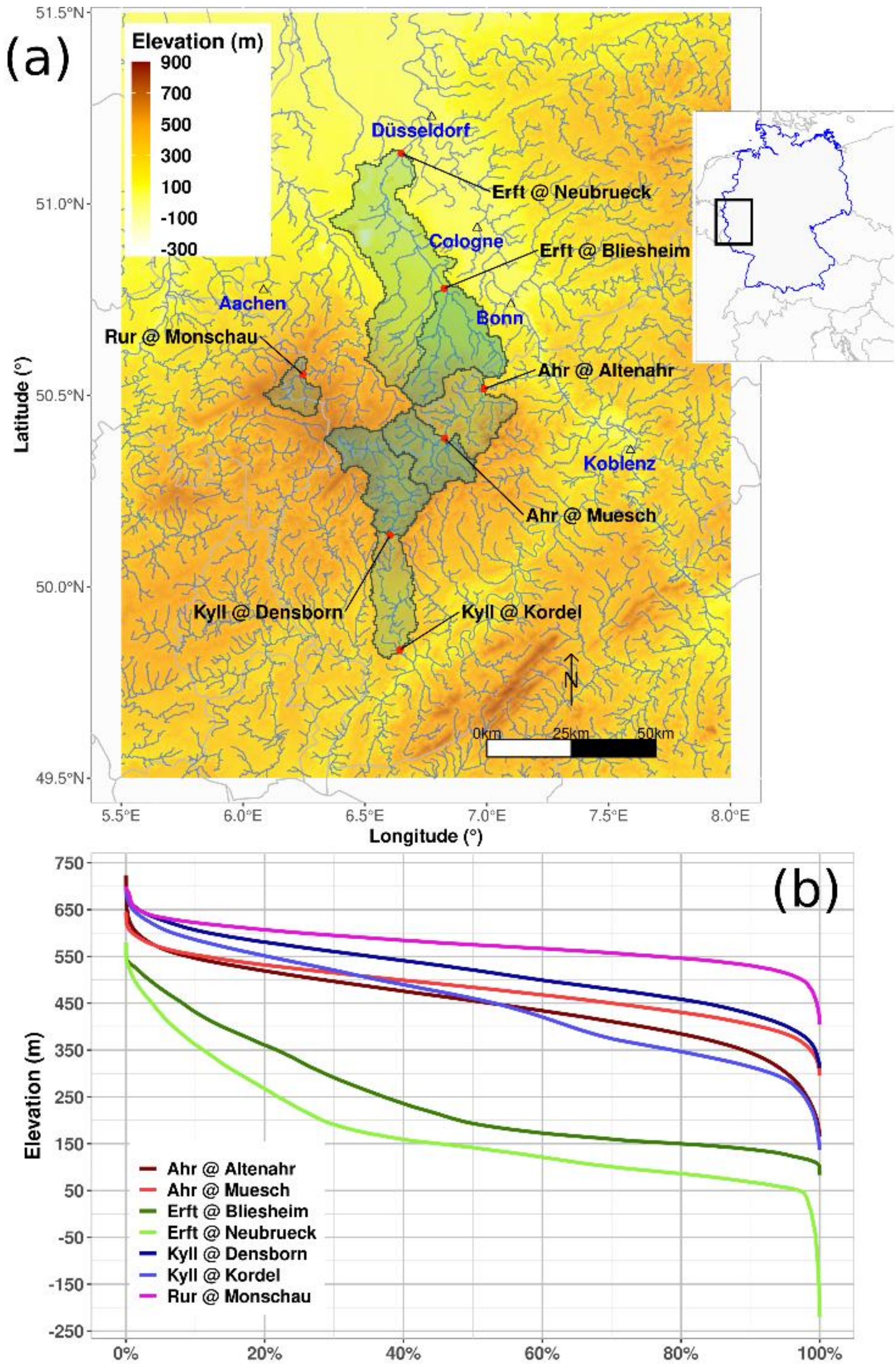


365

**Figure 1:** (a) Location of study region and (b) hypsometry of the seven catchments. Negative elevations are due to open-pit mines in the region.

https://doi.org/10.5194/nhess-2022-111
Preprint. Discussion started: 11 April 2022

Natural Hazards and Earth System Sciences
Discussions

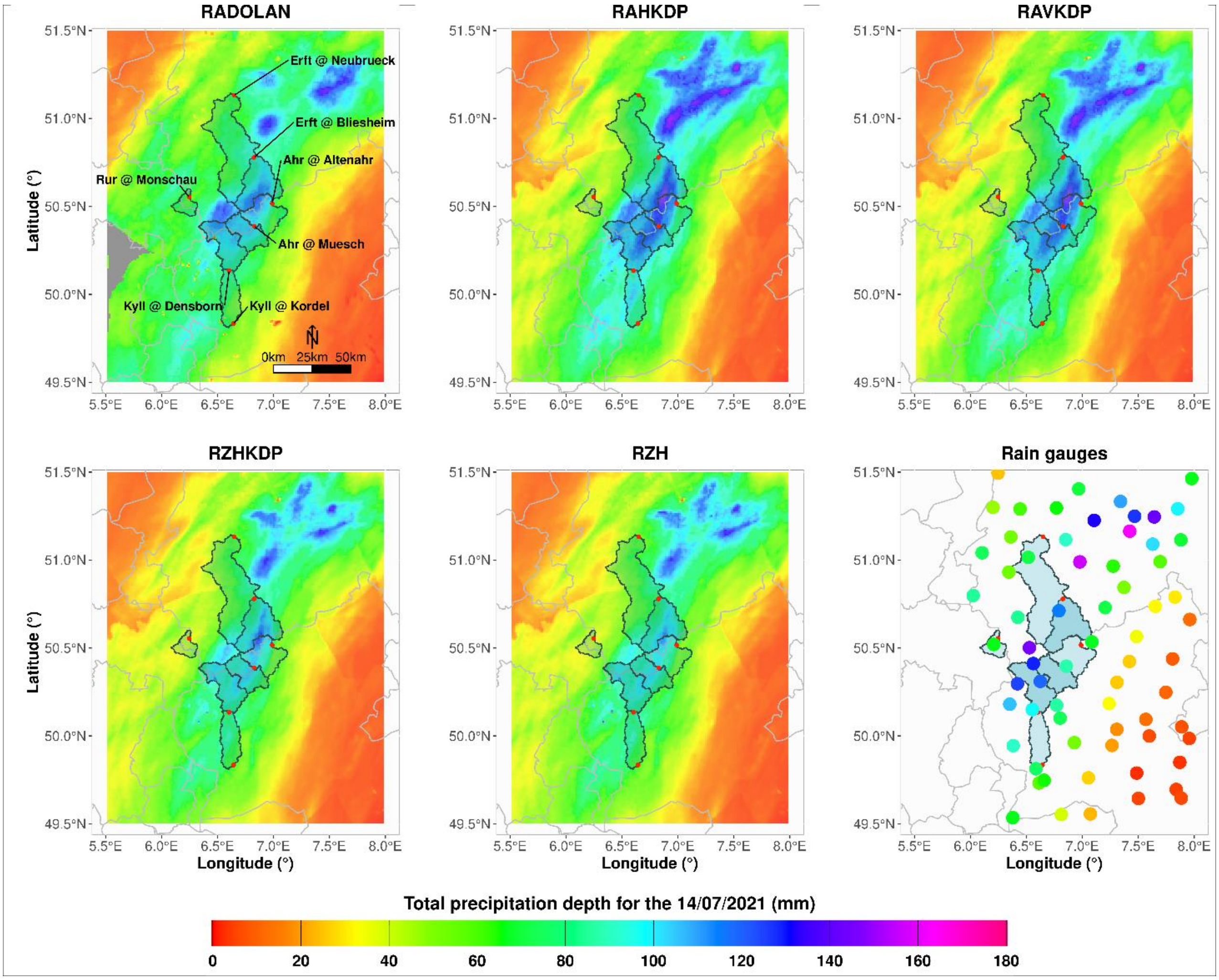


**Figure 2:** Total precipitation depths for the 14 July 2021 from the six QPE products (Table 2) over the study region.

https://doi.org/10.5194/nhess-2022-111
Preprint. Discussion started: 11 April 2022



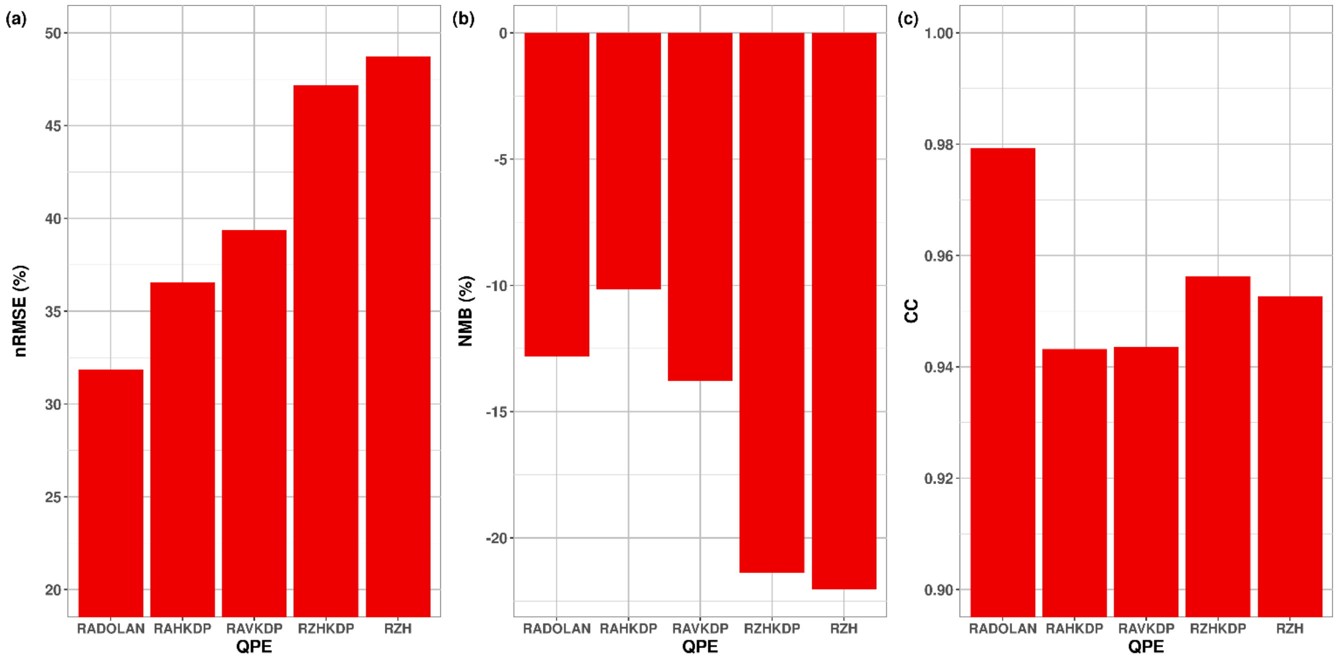


**Figure 3:** Point-scale evaluation scores of radar-based QPE with respect to ground-based measurements of total precipitation depth of the 14 July 2021.

375

https://doi.org/10.5194/nhess-2022-111
Preprint. Discussion started: 11 April 2022




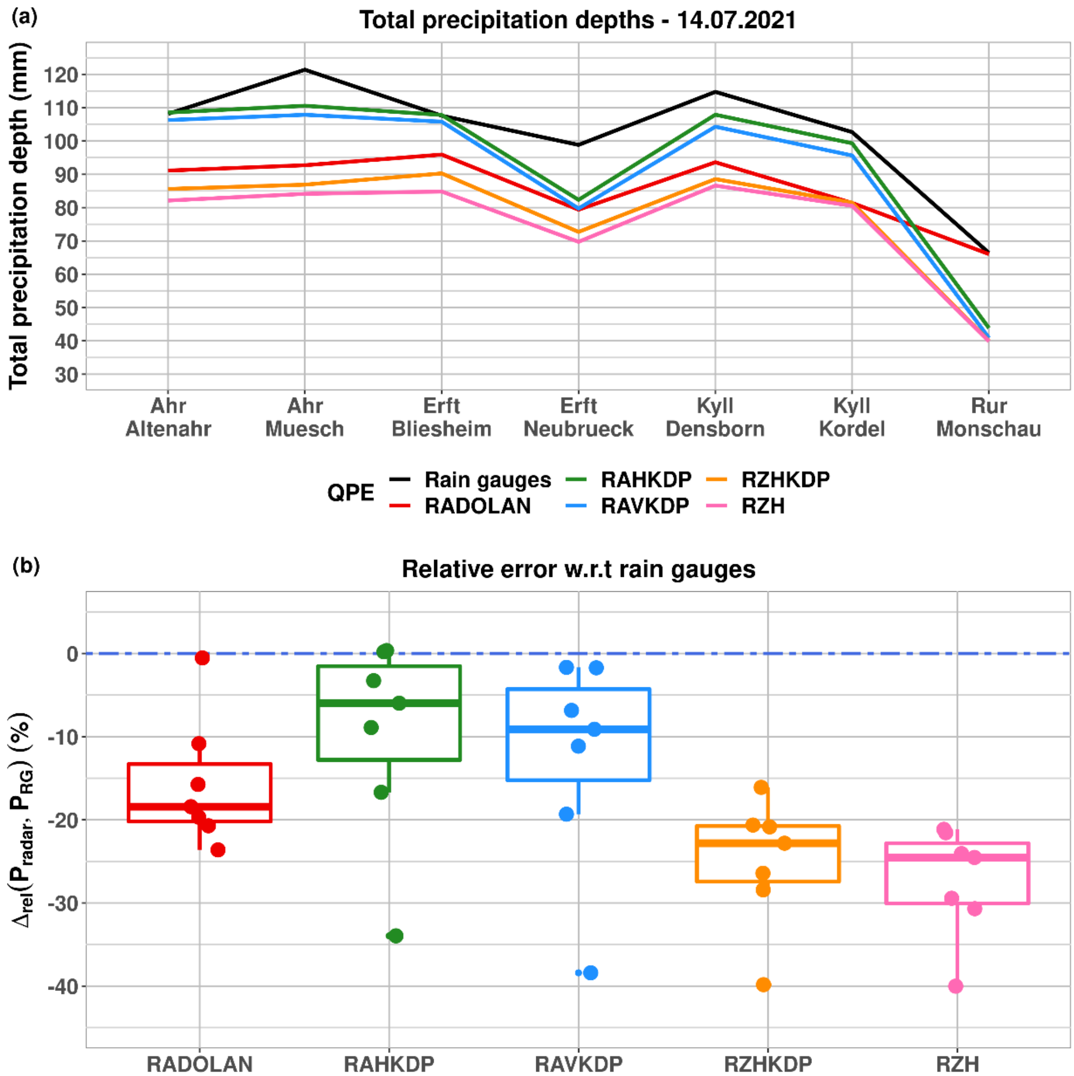


**Figure 4:** (a) Total precipitation depths for the 14 July 2021 estimated by rain gauges and QPE products. (b) Catchment-scale evaluation scores of radar-based QPE with respect to ground-based measurements of total precipitation depth of the 14 July 2021.

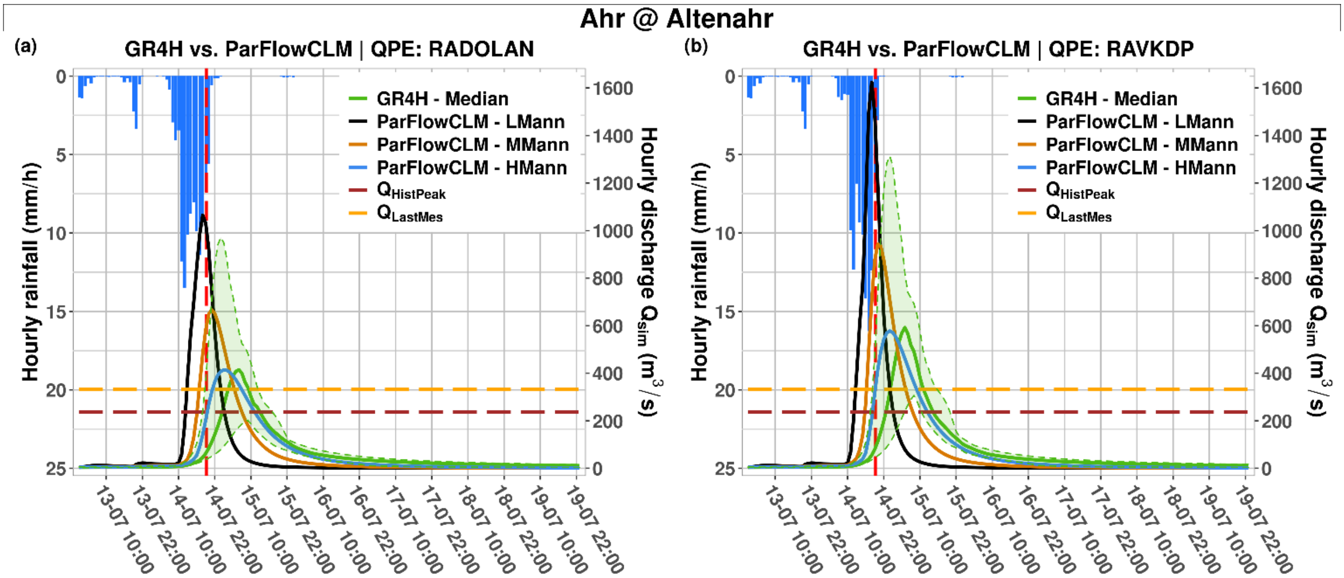


380

**Figure 5:** Simulated hydrographs by GR4H (in green) and ParFlowCLM (with low Manning's coefficient in black, medium Manning's coefficient in dark orange, and high Manning's coefficient in blue) using (a) RADOLAN and (b) RAVKDP as precipitation input for the Ahr at Altenahr. The dark red dashed line indicates the highest measured peakflow before July 2021. The orange dashed line indicates the last measured flow before measurement devices became unavailable, and the red dashed line its timing.

385

Natural Hazards and Earth System Sciences
Open Access
EGU
Discussions

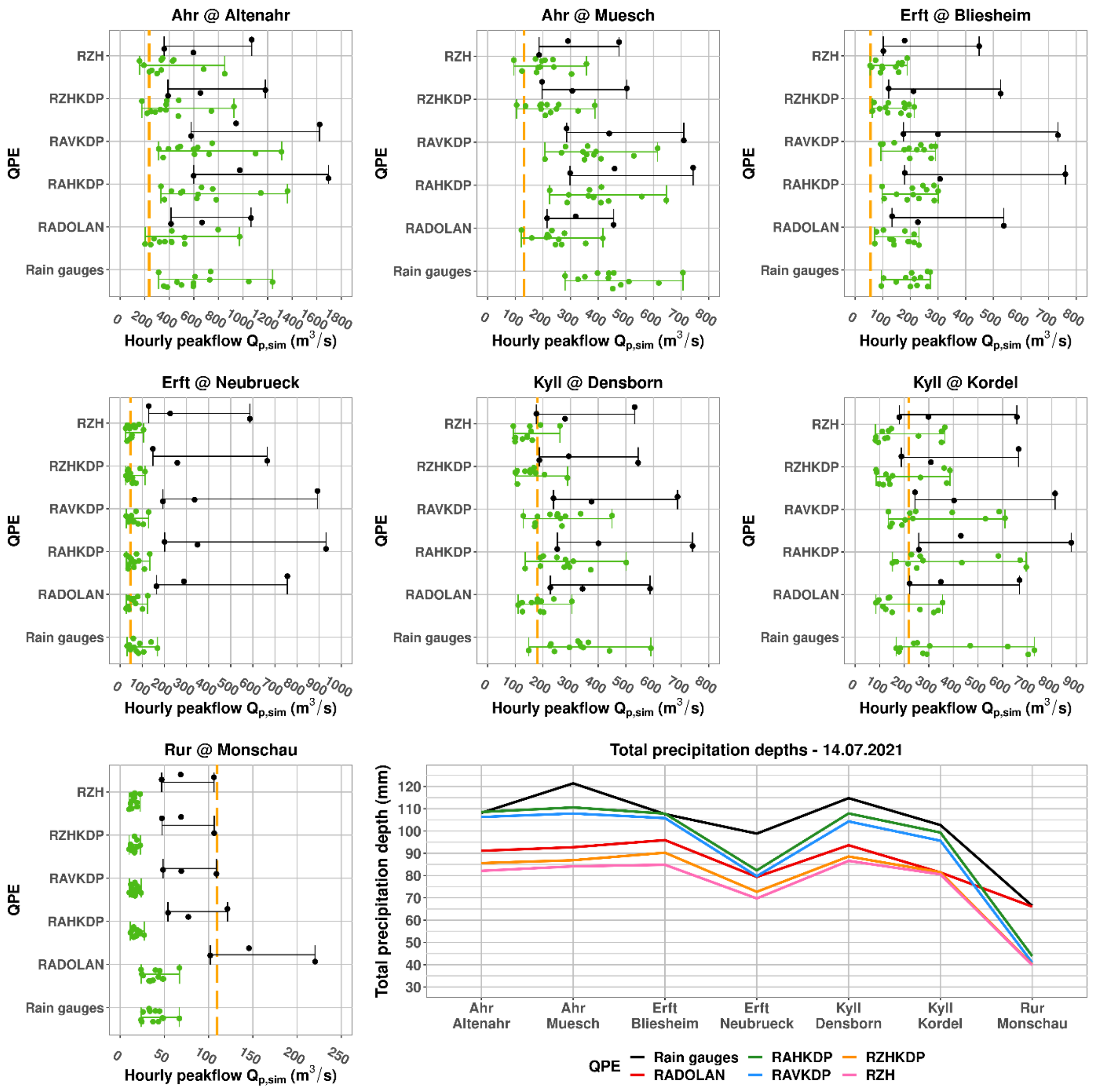


**Figure 6:** Distributions of simulated peakflows by GR4H (in green) and ParFlowCLM (in black) using six QPE inputs (on y-axis) for the seven catchments. Orange dashed lines indicate the highest measured peakflow before July 2021.

Natural Hazards and Earth System Sciences
Open Access
EGU
Discussions

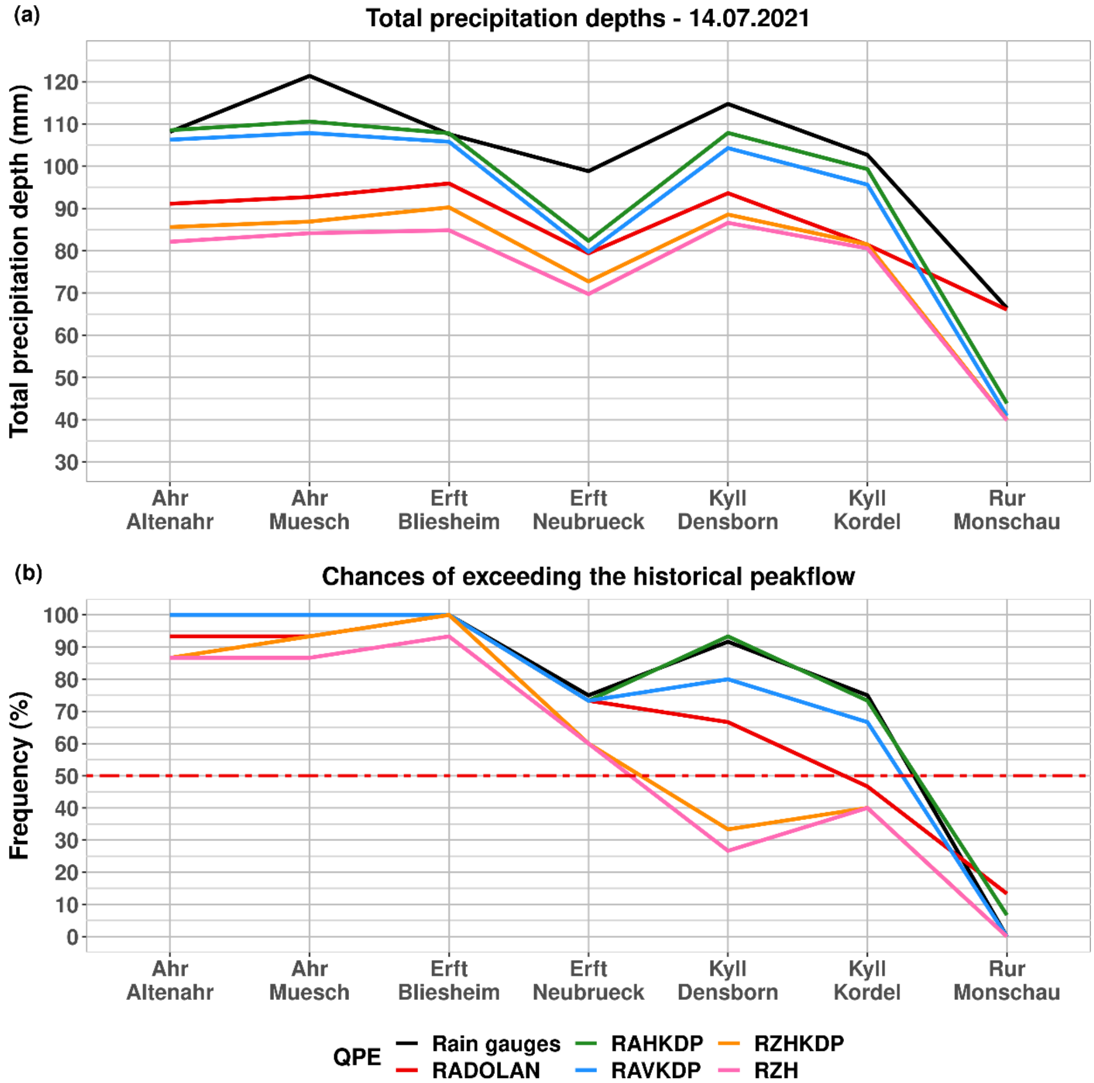


390

**Figure 7:** (a) Total precipitation depth for the 14 July 2021 from the six QPE products for each of the seven catchments and (b) resulting chances of overpassing the highest measured peakflow prior to July 2021.

https://doi.org/10.5194/nhess-2022-111
Preprint. Discussion started: 11 April 2022



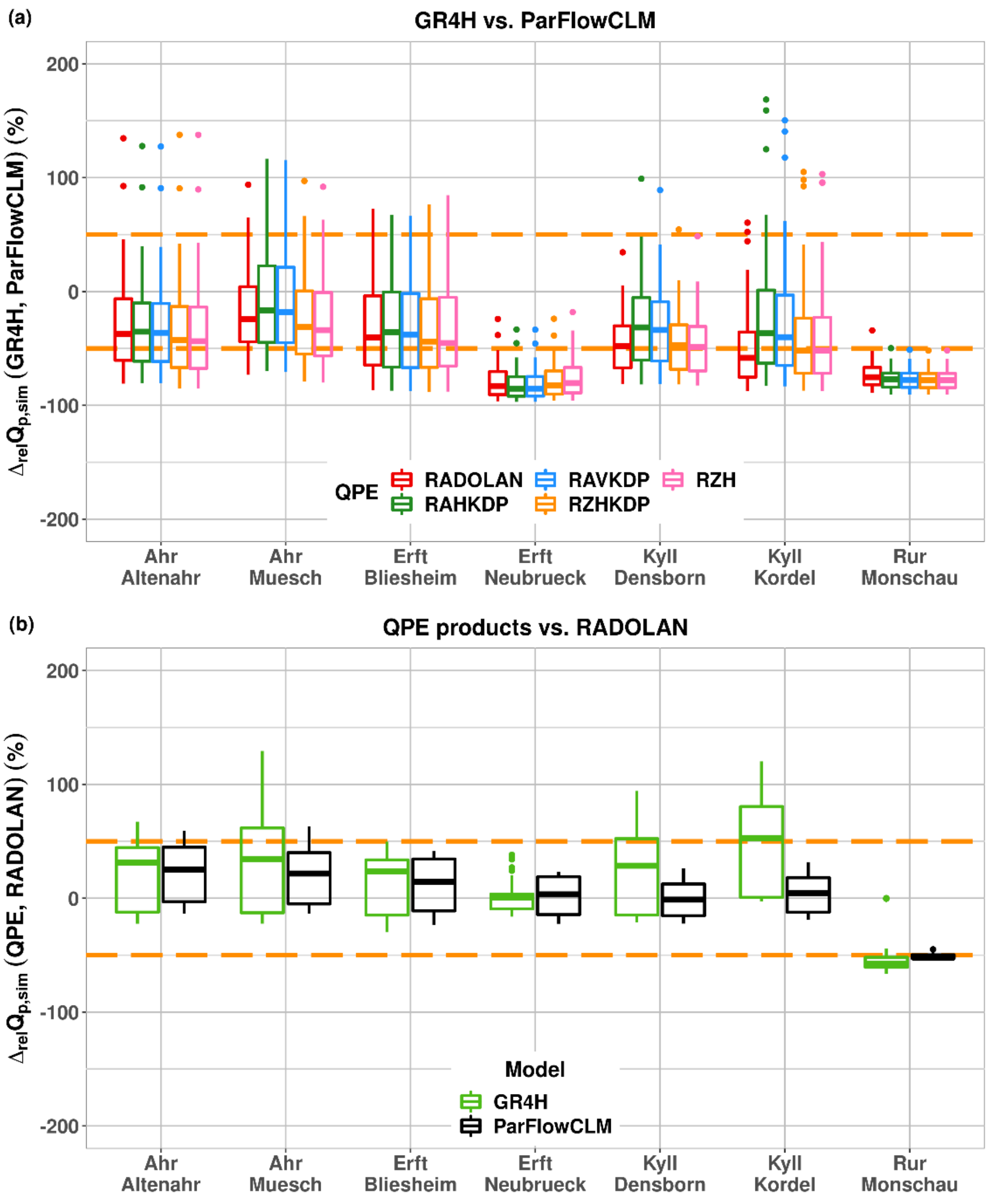


395 **Figure 8:** Relative errors in simulated peakflow due to (a) applying GR4H instead of ParFlowCLM across all QPE products, and to (b) replacing RADOLAN by any of the remaining five QPE products (Table 2) as precipitation input for the July 2021 event. Orange dashed lines limit the 50% relative error region.

Natural Hazards and Earth System Sciences Discussions

## References

Anagnostou, M. N., Kalogiros, J., Anagnostou, E. N., Tarolli, M., Papadopoulos, A., and Borga, M.: Performance evaluation of high-resolution rainfall estimation by X-band dual-polarization radar for flash flood applications in mountainous basins, Journal of Hydrology, 394, 4–16, https://doi.org/10.1016/j.jhydrol.2010.06.026, 2010.

Anagnostou, M. N., Nikolopoulos, E. I., Kalogiros, J., Anagnostou, E. N., Marra, F., Mair, E., Bertoldi, G., Tappeiner, U., and Borga, M.: Advancing Precipitation Estimation and Streamflow Simulations in Complex Terrain with X-Band Dual-Polarization Radar Observations, 10, 1258, https://doi.org/10.3390/rs10081258, 2018.

Anctil, F. and Ramos, M.-H.: Verification Metrics for Hydrological Ensemble Forecasts, in: Handbook of Hydrometeorological Ensemble Forecasting, edited by: Duan, Q., Pappenberger, F., Thielen, J., Wood, A., Cloke, H. L., and Schaake, J. C., Springer, Berlin, Heidelberg, 1–30, https://doi.org/10.1007/978-3-642-40457-3_3-1, 2017.

Anquetin, S., Yates, E., Ducrocq, V., Samouillan, S., Chancibault, K., Davolio, S., Accadia, C., Casaioli, M., Mariani, S., Ficca, G., Gozzini, B., Pasi, F., Pasqui, M., Garcia, A., Martorell, M., Romero, R., and Chessa, P.: The 8 and 9 September 2002 flash flood event in France: a model intercomparison, Nat. Hazards Earth Syst. Sci., 5, 741–754, https://doi.org/10.5194/nhess-5-741-2005, 2005.

Berne, A. and Krajewski, W. F.: Radar for hydrology: Unfulfilled promise or unrecognized potential?, Advances in Water Resources, 51, 357–366, https://doi.org/10.1016/j.advwatres.2012.05.005, 2013.

Borga, M., Boscolo, P., Zanon, F., and Sangati, M.: Hydrometeorological Analysis of the 29 August 2003 Flash Flood in the Eastern Italian Alps, 8, 1049–1067, https://doi.org/10.1175/JHM593.1, 2007.

Boushaki, F. I., Hsu, K.-L., Sorooshian, S., Park, G.-H., Mahani, S., and Shi, W.: Bias Adjustment of Satellite Precipitation Estimation Using Ground-Based Measurement: A Case Study Evaluation over the Southwestern United States, 10, 1231–1242, https://doi.org/10.1175/2009JHM1099.1, 2009.

Braud, I., Roux, H., Anquetin, S., Maubourguet, M.-M., Manus, C., Viallet, P., and Dartus, D.: The use of distributed hydrological models for the Gard 2002 flash flood event: Analysis of associated hydrological processes, Journal of Hydrology, 394, 162–181, https://doi.org/10.1016/j.jhydrol.2010.03.033, 2010.

Chen, J.-Y., Trömel, S., Ryzhkov, A., and Simmer, C.: Assessing the Benefits of Specific Attenuation for Quantitative Precipitation Estimation with a C-Band Radar Network, 22, 2617–2631, https://doi.org/10.1175/JHM-D-20-0299.1, 2021.

Cole, S. J. and Moore, R. J.: Distributed hydrological modelling using weather radar in gauged and ungauged basins, Advances in Water Resources, 32, 1107–1120, https://doi.org/10.1016/j.advwatres.2009.01.006, 2009.

Coron, L., Thirel, G., Delaigue, O., Perrin, C., and Andréassian, V.: The suite of lumped GR hydrological models in an R package, 94, 166–171, https://doi.org/10.1016/j.envsoft.2017.05.002, 2017.

Cunha, L. K., Smith, J. A., Krajewski, W. F., Baeck, M. L., and Seo, B.-C.: NEXRAD NWS Polarimetric Precipitation Product Evaluation for IFloodS, 16, 1676–1699, https://doi.org/10.1175/JHM-D-14-0148.1, 2015.

Derin, Y., Anagnostou, E., Anagnostou, M., and Kalogiros, J.: Evaluation of X-Band Dual-Polarization Radar-Rainfall Estimates from OLYMPEX, 20, 1941–1959, https://doi.org/10.1175/JHM-D-19-0097.1, 2019.

https://doi.org/10.5194/nhess-2022-111
Preprint. Discussion started: 11 April 2022

Natural Hazards and Earth System Sciences
Open Access
Discussions

Deutsche Welle: German floods: Climate change made heavy rains in Europe more likely: https://www.dw.com/en/german-floods-climate-change/a-58959677, last access: 16 February 2022, 2021.

Diederich, M., Ryzhkov, A., Simmer, C., Zhang, P., and Trömel, S.: Use of Specific Attenuation for Rainfall Measurement at X-Band Radar Wavelengths. Part I: Radar Calibration and Partial Beam Blockage Estimation, 16, 487–502, https://doi.org/10.1175/JHM-D-14-0066.1, 2015a.

Diederich, M., Ryzhkov, A., Simmer, C., Zhang, P., and Trömel, S.: Use of Specific Attenuation for Rainfall Measurement at X-Band Radar Wavelengths. Part II: Rainfall Estimates and Comparison with Rain Gauges, 16, 503–516, https://doi.org/10.1175/JHM-D-14-0067.1, 2015b.

Dottori, F., Szewczyk, W., Ciscar, J.-C., Zhao, F., Alfieri, L., Hirabayashi, Y., Bianchi, A., Mongelli, I., Frieler, K., Betts, R. A., and Feyen, L.: Increased human and economic losses from river flooding with anthropogenic warming, Nature Clim Change, 8, 781–786, https://doi.org/10.1038/s41558-018-0257-z, 2018.

Dougherty, E. and Rasmussen, K. L.: Changes in Future Flash Flood–Producing Storms in the United States, 21, 2221–2236, https://doi.org/10.1175/JHM-D-20-0014.1, 2020.

Dumont, M., Saadi, M., Oudin, L., Lachassagne, P., Nugraha, B., Fadillah, A., Bonjour, J.-L., Muhammad, A., Hendarmawan, Dörfliger, N., and Plagnes, V.: Assessing rainfall global products reliability for water resource management in a tropical volcanic mountainous catchment, Journal of Hydrology: Regional Studies, 40, 101037, https://doi.org/10.1016/j.ejrh.2022.101037, 2022.

Duscher, K., Günther, A., Richts, A., Clos, P., Philipp, U., and Struckmeier, W.: The GIS layers of the "International Hydrogeological Map of Europe 1:1,500,000" in a vector format, Hydrogeol J, 23, 1867–1875, https://doi.org/10.1007/s10040-015-1296-4, 2015.

Edijatno, Nascimento, N. de O., Yang, X., Makhlouf, Z., and Michel, C.: GR3J: a daily watershed model with three free parameters, 44, 263–277, https://doi.org/10.1080/02626669909492221, 1999.

Emmanuel, I., Payrastre, O., Andrieu, H., and Zuber, F.: A method for assessing the influence of rainfall spatial variability on hydrograph modeling. First case study in the Cevennes Region, southern France, Journal of Hydrology, 555, 314–322, https://doi.org/10.1016/j.jhydrol.2017.10.011, 2017.

Ficchì, A., Perrin, C., and Andréassian, V.: Hydrological modelling at multiple sub-daily time steps: Model improvement via flux-matching, Journal of Hydrology, 575, 1308–1327, https://doi.org/10.1016/j.jhydrol.2019.05.084, 2019.

Fowler, H. J., Lenderink, G., Prein, A. F., Westra, S., Allan, R. P., Ban, N., Barbero, R., Berg, P., Blenkinsop, S., Do, H. X., Guerreiro, S., Haerter, J. O., Kendon, E. J., Lewis, E., Schaer, C., Sharma, A., Villarini, G., Wasko, C., and Zhang, X.: Anthropogenic intensification of short-duration rainfall extremes, Nat Rev Earth Environ, 2, 107–122, https://doi.org/10.1038/s43017-020-00128-6, 2021.

GDV: Die sieben schwersten Überschwemmungen: https://www.gdv.de/resource/blob/68972/8beef4662785206438081c2c5f502d0e/download-die-sieben-schwersten-ueberschwemmungen-data.pdf, last access: 9 February 2022, 2021.

Gourley, J. J., Giangrande, S. E., Hong, Y., Flamig, Z. L., Schuur, T., and Vrugt, J. A.: Impacts of Polarimetric Radar Observations on Hydrologic Simulation, 11, 781–796, https://doi.org/10.1175/2010JHM1218.1, 2010.

https://doi.org/10.5194/nhess-2022-111
Preprint. Discussion started: 11 April 2022


Natural Hazards and Earth System Sciences
Discussions

Gupta, H. V., Kling, H., Yilmaz, K. K., and Martinez, G. F.: Decomposition of the mean squared error and NSE performance criteria: Implications for improving hydrological modelling, Journal of Hydrology, 377, 80–91, https://doi.org/10.1016/j.jhydrol.2009.08.003, 2009.

Hapuarachchi, H. a. P., Wang, Q. J., and Pagano, T. C.: A review of advances in flash flood forecasting, 25, 2771–2784, https://doi.org/10.1002/hyp.8040, 2011.

Harrison, D. L., Driscoll, S. J., and Kitchen, M.: Improving precipitation estimates from weather radar using quality control and correction techniques, Meteorol. App., 7, 135–144, https://doi.org/10.1017/S1350482700001468, 2000.

He, X., Koch, J., Zheng, C., Bøvith, T., and Jensen, K. H.: Comparison of Simulated Spatial Patterns Using Rain Gauge and Polarimetric-Radar-Based Precipitation Data in Catchment Hydrological Modeling, 19, 1273–1288, https://doi.org/10.1175/JHM-D-17-0235.1, 2018.

Hengl, T., Jesus, J. M. de, Heuvelink, G. B. M., Gonzalez, M. R., Kilibarda, M., Blagotić, A., Shangguan, W., Wright, M. N., Geng, X., Bauer-Marschallinger, B., Guevara, M. A., Vargas, R., MacMillan, R. A., Batjes, N. H., Leenaars, J. G. B., Ribeiro, E., Wheeler, I., Mantel, S., and Kempen, B.: SoilGrids250m: Global gridded soil information based on machine learning, PLOS ONE, 12, e0169748, https://doi.org/10.1371/journal.pone.0169748, 2017.

Huang, Y., Bárdossy, A., and Zhang, K.: Sensitivity of hydrological models to temporal and spatial resolutions of rainfall data, 23, 2647–2663, https://doi.org/10.5194/hess-23-2647-2019, 2019.

Junghänel, T., Bissolli, P., Daßler, J., Fleckenstein, R., Imbery, F., Janssen, W., Lengfeld, K., Leppelt, T., Rauthe, M., Rauthe-Schöch, A., Rocek, M., Walawender, E., and Weigl, E.: Hydro-klimatologische Einordnung der Stark- und Dauerniederschläge in Teilen Deutschlands im Zusammenhang mit dem Tiefdruckgebiet „Bernd“ vom 12. bis 19. Juli 202, 16, 2021.

Kendon, E. J., Roberts, N. M., Fowler, H. J., Roberts, M. J., Chan, S. C., and Senior, C. A.: Heavier summer downpours with climate change revealed by weather forecast resolution model, Nature Clim Change, 4, 570–576, https://doi.org/10.1038/nclimate2258, 2014.

Kollet, S. J. and Maxwell, R. M.: Integrated surface–groundwater flow modeling: A free-surface overland flow boundary condition in a parallel groundwater flow model, Advances in Water Resources, 29, 945–958, https://doi.org/10.1016/j.advwatres.2005.08.006, 2006.

Kreienkamp, F., Philip, S. Y., Tradowsky, J. S., Kew, S. F., Lorenz, P., Arrighi, J., Belleflamme, A., Bettmann, T., Caluwaerts, S., Chan, S. C., Ciavarella, A., De Cruz, L., de Vries, H., Demuth, N., Ferrone, A., Fischer, rich M., Fowler, H. J., Goergen, K., Heinrich, D., Henrichs, Y., Lenderink, G., Kaspar, F., Nilson, E., Otto, F. E. L., Ragone, F., Seneviratne, S. I., Singh, R. K., Skålevåg, A., Termonia, P., Thalheimer, L., van Aalst, M., Van den Bergh, J., Van de Vyver, H., Vannitsem, S., van Oldenborgh, G. J., Van Schaeybroeck, B., Vautard, R., Vonk, D., and Wanders, N.: Rapid attribution of heavy rainfall events leading to the severe flooding in Western Europe during July 2021, 2021.

Kuczera, G., Kavetski, D., Franks, S., and Thyer, M.: Towards a Bayesian total error analysis of conceptual rainfall-runoff models: Characterising model error using storm-dependent parameters, Journal of Hydrology, 331, 161–177, https://doi.org/10.1016/j.jhydrol.2006.05.010, 2006.

Kuffour, B. N. O., Engdahl, N. B., Woodward, C. S., Condon, L. E., Kollet, S., and Maxwell, R. M.: Simulating coupled surface–subsurface flows with ParFlow v3.5.0: capabilities, applications, and ongoing development of an open-source, massively parallel, integrated hydrologic model, 13, 1373–1397, https://doi.org/10.5194/gmd-13-1373-2020, 2020.

https://doi.org/10.5194/nhess-2022-111
Preprint. Discussion started: 11 April 2022




Langanke, T., Steidl, M., Schleicher, C., and Sannier, C.: Copernicus Land Monitoring Service – High Resolution Layer Imperviousness: Product Specifications Document, European Environment Agency, 2016.

Lin, P., Hopper, L. J., Yang, Z.-L., Lenz, M., and Zeitler, J. W.: Insights into Hydrometeorological Factors Constraining Flood Prediction Skill during the May and October 2015 Texas Hill Country Flood Events, 19, 1339–1361, https://doi.org/10.1175/JHM-D-18-0038.1, 2018.

Lobligeois, F., Andréassian, V., Perrin, C., Tabary, P., and Loumagne, C.: When does higher spatial resolution rainfall information improve streamflow simulation? An evaluation using 3620 flood events, 18, 575–594, https://doi.org/10.5194/hess-18-575-2014, 2014.

Lumbroso, D. and Gaume, E.: Reducing the uncertainty in indirect estimates of extreme flash flood discharges, Journal of Hydrology, 414–415, 16–30, https://doi.org/10.1016/j.jhydrol.2011.08.048, 2012.

Marshall, J. S. and Palmer, W. M. K.: The distribution of raindrops with size, 5, 165–166, https://doi.org/10.1175/1520-0469(1948)005<0165:TDORWS>2.0.CO;2, 1948.

Maxwell, R. M.: A terrain-following grid transform and preconditioner for parallel, large-scale, integrated hydrologic modeling, Advances in Water Resources, 53, 109–117, https://doi.org/10.1016/j.advwatres.2012.10.001, 2013.

Muñoz-Sabater, J., Dutra, E., Agustí-Panareda, A., Albergel, C., Arduini, G., Balsamo, G., Boussetta, S., Choulga, M., Harrigan, S., Hersbach, H., Martens, B., Miralles, D. G., Piles, M., Rodríguez-Fernández, N. J., Zsoter, E., Buontempo, C., and Thépaut, J.-N.: ERA5-Land: a state-of-the-art global reanalysis dataset for land applications, 13, 4349–4383, https://doi.org/10.5194/essd-13-4349-2021, 2021.

Nash, J. E. and Sutcliffe, J. V.: River flow forecasting through conceptual models part I — A discussion of principles, Journal of Hydrology, 10, 282–290, https://doi.org/10.1016/0022-1694(70)90255-6, 1970.

Nissen, K. M. and Ulbrich, U.: Increasing frequencies and changing characteristics of heavy precipitation events threatening infrastructure in Europe under climate change, 17, 1177–1190, https://doi.org/10.5194/nhess-17-1177-2017, 2017.

Oudin, L., Perrin, C., Mathevet, T., Andréassian, V., and Michel, C.: Impact of biased and randomly corrupted inputs on the efficiency and the parameters of watershed models, Journal of Hydrology, 320, 62–83, https://doi.org/10.1016/j.jhydrol.2005.07.016, 2006.

Park, S., Berenguer, M., and Sempere-Torres, D.: Long-term analysis of gauge-adjusted radar rainfall accumulations at European scale, Journal of Hydrology, 573, 768–777, https://doi.org/10.1016/j.jhydrol.2019.03.093, 2019.

Pechlivanidis, I. G., McIntyre, N., and Wheater, H. S.: The significance of spatial variability of rainfall on simulated runoff: an evaluation based on the Upper Lee catchment, UK, Hydrology Research, 48, 1118–1130, https://doi.org/10.2166/nh.2016.038, 2016.

Perrin, C., Michel, C., and Andréassian, V.: Improvement of a parsimonious model for streamflow simulation, Journal of Hydrology, 279, 275–289, https://doi.org/10.1016/S0022-1694(03)00225-7, 2003.

Pokhrel, P. and Gupta, H. V.: On the ability to infer spatial catchment variability using streamflow hydrographs, 47, https://doi.org/10.1029/2010WR009873, 2011.

Poméon, T., Wagner, N., Furusho, C., Kollet, S., and Reinoso-Rondinel, R.: Performance of a PDE-Based Hydrologic Model in a Flash Flood Modeling Framework in Sparsely-Gauged Catchments, 12, 2157, https://doi.org/10.3390/w12082157, 2020.

Raimonet, M., Oudin, L., Thieu, V., Silvestre, M., Vautard, R., Rabouille, C., and Moigne, P. L.: Evaluation of Gridded Meteorological Datasets for Hydrological Modeling, 18, 3027–3041, https://doi.org/10.1175/JHM-D-17-0018.1, 2017.

Renard, B., Kavetski, D., Leblois, E., Thyer, M., Kuczera, G., and Franks, S. W.: Toward a reliable decomposition of predictive uncertainty in hydrological modeling: Characterizing rainfall errors using conditional simulation, 47, https://doi.org/10.1029/2011WR010643, 2011.

Ryzhkov, A., Diederich, M., Zhang, P., and Simmer, C.: Potential Utilization of Specific Attenuation for Rainfall Estimation, Mitigation of Partial Beam Blockage, and Radar Networking, 31, 599–619, https://doi.org/10.1175/JTECH-D-13-00038.1, 2014.

Ryzhkov, A. V., Schuur, T. J., Burgess, D. W., Heinselman, P. L., Giangrande, S. E., and Zrnic, D. S.: The Joint Polarization Experiment: Polarimetric Rainfall Measurements and Hydrometeor Classification, 86, 809–824, https://doi.org/10.1175/BAMS-86-6-809, 2005.

Saulnier, G.-M. and Le Lay, M.: Sensitivity of flash-flood simulations on the volume, the intensity, and the localization of rainfall in the Cévennes-Vivarais region (France), 45, https://doi.org/10.1029/2008WR006906, 2009.

Schaap, M. G., Leij, F. J., and van Genuchten, M. Th.: rosetta : a computer program for estimating soil hydraulic parameters with hierarchical pedotransfer functions, Journal of Hydrology, 251, 163–176, https://doi.org/10.1016/S0022-1694(01)00466-8, 2001.

Schalge, B., Haefliger, V., Kollet, S., and Simmer, C.: Improvement of surface run-off in the hydrological model ParFlow by a scale-consistent river parameterization, 33, 2006–2019, https://doi.org/10.1002/hyp.13448, 2019.

Schleiss, M., Olsson, J., Berg, P., Niemi, T., Kokkonen, T., Thorndahl, S., Nielsen, R., Ellerbæk Nielsen, J., Bozhinova, D., and Pulkkinen, S.: The accuracy of weather radar in heavy rain: a comparative study for Denmark, the Netherlands, Finland and Sweden, Hydrol. Earth Syst. Sci., 24, 3157–3188, https://doi.org/10.5194/hess-24-3157-2020, 2020.

Singh, H. and Reza Najafi, M.: Evaluation of gridded climate datasets over Canada using univariate and bivariate approaches: Implications for hydrological modelling, Journal of Hydrology, 584, 124673, https://doi.org/10.1016/j.jhydrol.2020.124673, 2020.

Sokol, Z., Szturc, J., Orellana-Alvear, J., Popová, J., Jurczyk, A., and Célleri, R.: The Role of Weather Radar in Rainfall Estimation and Its Application in Meteorological and Hydrological Modelling—A Review, 13, 351, https://doi.org/10.3390/rs13030351, 2021.

Staatliches Umweltamt Köln: Ergebnisbericht Erft. Wasserrahmenrichtlinie in NRW – Bestandsaufnahme, Ministerium fuer Umwelt und Naturschutz, Landwirtschaft und Verbraucherschutz des Landes Nordrhein-Westfalen, 2005.

Tetzlaff, D. and Uhlenbrook, S.: Significance of spatial variability in precipitation for process-oriented modelling: results from two nested catchments using radar and ground station data, 9, 29–41, https://doi.org/10.5194/hess-9-29-2005, 2005.

Trenberth, K.: Changes in precipitation with climate change, Clim. Res., 47, 123–138, https://doi.org/10.3354/cr00953, 2011.

Yamazaki, D., Ikeshima, D., Sosa, J., Bates, P. D., Allen, G. H., and Pavelsky, T. M.: MERIT Hydro: A High-Resolution Global Hydrography Map Based on Latest Topography Dataset, 55, 5053–5073, https://doi.org/10.1029/2019WR024873, 2019.

https://doi.org/10.5194/nhess-2022-111
Preprint. Discussion started: 11 April 2022

Natural Hazards and Earth System Sciences Discussions

Zappa, M., Jaun, S., Germann, U., Walser, A., and Fundel, F.: Superposition of three sources of uncertainties in operational flood forecasting chains, Atmospheric Research, 100, 246–262, https://doi.org/10.1016/j.atmosres.2010.12.005, 2011.

Zhou, Z., Smith, J. A., Yang, L., Baeck, M. L., Chaney, M., Veldhuis, M.-C. T., Deng, H., and Liu, S.: The complexities of urban flood response: Flood frequency analyses for the Charlotte metropolitan region, 53, 7401–7425, https://doi.org/10.1002/2016WR019997, 2017.